GEOLOGICAL SURVEY OF CANADA
OPEN FILE 7465

A Magnetotelluric Survey and Preliminary Geophysical Inversion and Visualization of the NICO IOCG deposit, Northwest Territories

J.A Craven, B.J. Roberts, N. Hayward, M. Stefanescu, L. Corriveau

2013

Natural Resources Canada | Ressources naturelles Canada

Canada

GEOLOGICAL SURVEY OF CANADA
OPEN FILE 7465

A Magnetotelluric Survey and Preliminary Geophysical Inversion and Visualization of the NICO IOCG deposit, Northwest Territories

J.A Craven, B.J. Roberts, N. Hayward, M. Stefanescu, L. Corriveau

2013

doi:10.4095/292869

This publication is available for free download through GEOSCAN (http://geoscan.ess.nrcan.gc.ca/).

Recommended citation
Craven, J.A., Roberts, B.J., Hayward, N., Stefanescu, M., and Corriveau, M., 2013, A Magnetotelluric Survey and Preliminary Geophysical Inversion and Visualization of the NICO IOCG deposit, Northwest Terrirories; Geological Survey of Canada, Open File 7465, p. 25, doi:10.4095/292869

Abstract

Introduction

To improve our understanding of the NICO deposit and Iron Oxide-Copper-Gold (IOCG) deposits in general we conducted both a regional-scale (10's km) and mine-scale (a few km) magnetotelluric (MT) study at the NICO deposit in the summer of 2010. An MT study involves the measurement, along a profile or on a grid, of variations in the natural magnetic field and correlated changes in voltages in the ground due to so-called "telluric" currents. The data collected enable a view of the electrical resistivity structure from the surface to the depth of the mantle. The survey itself is relatively easy to conduct, requiring a crew of only 2 or 3 persons due to the simplicity of installing the receiver equipment and the fact that no artificial or man-made energy source needs to be installed.

The purpose of the MT survey is twofold. The first is to test the IOCG exploration model proposed by Corriveau et al (2010). The Corriveau et al alteration vector-to-mineralisation model enables effective exploration in a geologically complex region by providing a framework to understand the spatial and temporal relationships amongst the alteration products associated with the mineralization event (Corriveau et al., 2010). The model can be treated as a scientific hypothesis and tested. For example, Potter et al. (2013) have successfully tested the validity of the model to vector towards ore at the Fab lake showing. A fundamental result of Potter et al. (2012) is their demonstration that the model provides sufficient detail and tools that can be used by others to explore for ore. In this paper we test the spatial associations predicted by the model using geophysical methods due to the unique geophysical signatures alteration products in the model suggests. For example, sulphides should be conductive, but not magnetic. Magnetite should be magnetic, but not conductive. The second purpose of the MT work is more regional in nature. Regional MT studies (Heinson et al, 2006) and isotope studies at the Olympic Dam deposit (Johnson and McCulloch, 1995) have suggested a mantle source for mineralizing fluids. Seismic surveys (Drummond et al., 2006) support this notion by suggesting that deep faults or conduits beneath Olympic Dam permit mantle fluids access to the uppermost portions of the lithosphere. In addition, at Olympic Dam, the lithospheric architecture includes tapering out of an Archean lithospheric root, the extremity of which is directly under Olympic Dam (cf. Drummond et al., 2006; Cook et al., 1998; Snyder, 2008; Spratt et al., 2009). Whether similar roots and deep-seated conduits exist beneath the NICO deposit, and if there is evidence for large-scale fluid movement along them are key questions a regional MT survey can address.

Geological Setting

Multiple Paleoproterozoic accretion events and associated tectonothermal activity on the western side (present day) of the Archean Slave craton built the lithosphere into which IOCG mineralizing fluids percolated. During the interval between 1.88 and 1.84 Ga. a calc-alkaline volcano-plutonic arc (Great Bear magmatic zone, GBmz) developed along a continental convergent margin, itself a remnant of an earlier, ca. 2.1-1.88 Ga magmatic arc, the Hottah terrane (Hildebrand et al., 1987, 2010). Such interpretations supersede previous back-arc basin models (Hoffman and McGlynn, 1977) and Cook et al., 1998). The IOCG-type hydrothermal systems, coeval with volcano-plutonic activity, percolated within the length of the exposed GBmz. However, structural breccias and a few IOCG environments occur along, or to the east of, the Wopmay fault zone (e.g., Montreuil et al., 2009), mylonitic rocks

broken by a brittle fault system confined in a belt up to 20 km wide. Docking of the Fort Simpson terrane with the western margin of Hottah terrane at 1.84 Ga marks the end of magmatic activity in the GBmz and may have led to the creation of a network of northeast-trending dextral transcurrent faults dismembered apparently to upper mantle depths (Wu et al., 2005).

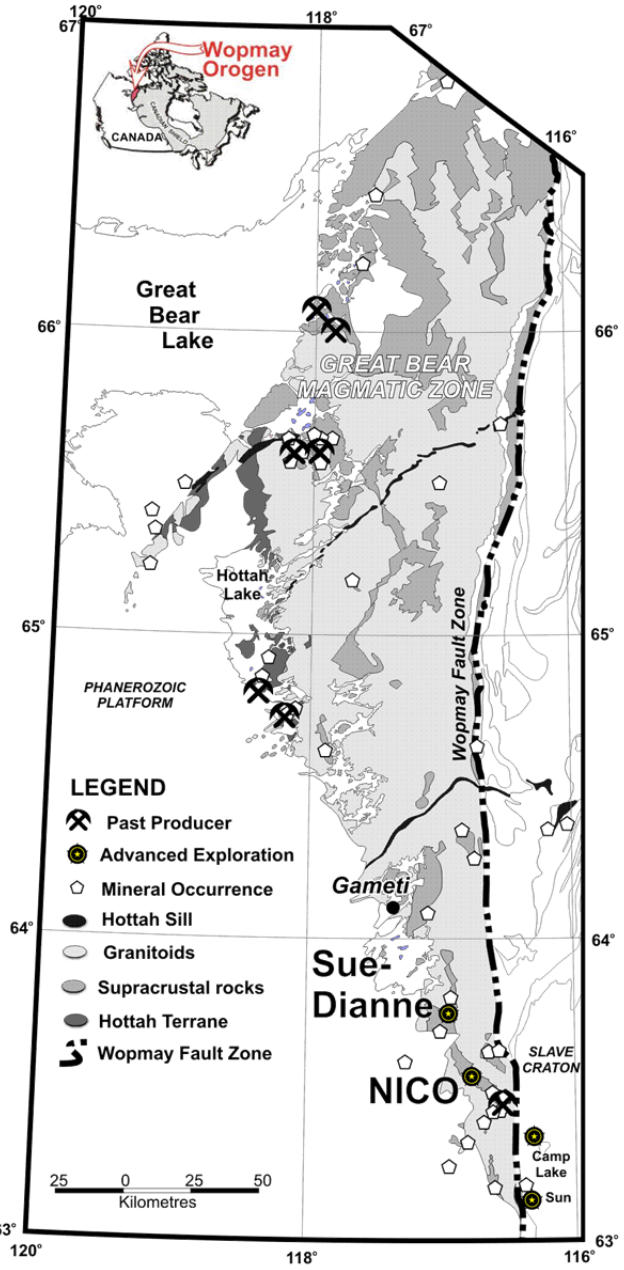

Figure 1. Regional geology and major mine camps (After Montreuil et al., 2010).

Evaluating the amount of reworked Archean crust in the basement of the GBmz is problematic. There is visible evidence of reworked Archean rocks of the Slave craton as far west as the Wopmay fault zone. Isotopic signatures do not record the presence of Archean crust under the GBmz (Hildebrand et al., 2010). Regional magnetotelluric studies (Spratt et al., 2009) to the north of the present study suggest the Slave craton has a resistive wedge-shaped Archean lithospheric root tapering downward to the west, nearly reaching at depth the location of the exposed segments of Hottah terrane. A resistive cratonic root imaged to depths of ca. 200 km also occurs below the Hottah terrane. Both roots are separated by a less resistive region beneath the Great Bear magmatic zone and the overall picture is

one of crustal wedging or 'crocodile' tectonics comparable to Paleoproterozoic orogens (Snyder, 2008) observed geophysically world-wide. In addition, currently known IOCG environments in the GBmz occur above some of the major lithospheric discontinuities observed by Spratt et al. (2009) north of the NICO deposit. A subsequent paper will address whether the spatially restricted regional MT survey observed similar features to exist beneath the NICO camp, and whether such features can be tied to those observed in the mine scale survey discussed in this paper.

The alteration vector-to-mineralisation model (Corriveau et al., 2010)

Common to all IOCG deposits are metalliferous zones within regional-scale hydrothermal alteration systems that comprise extensive, intense, and diagnostic sodic (albite or scapolite), calcic-ferrous (±sodic) (amphibole-magnetite), potassic-ferrous/ferric (biotite/K feldspar-magnetite) and/or potassic-ferric (K feldspar/sericite-hematite-chloritecarbonate) hydrothermal alteration zones. The alteration characteristics are not all necessarily present for any one deposit; however in general there is a fundamental spatio-temporal relationship as that summarized in Figure 2. At NICO, early sodic (±calcic) and calcic-ferrous (±sodic) (magnetite) alteration zones are commonly laterally extensive and rich in albite and amphibole-magnetite±apatite respectively. They occurred after an extensive brecciiation event (Montreuil et al., 2010) observed within a 3 x 0.5 km wide corridor located approximately one kilometer south of NICO. These alteration zones are clear indicators of prospective regions that may host iron-oxide apatite (IOA) deposits. More importantly, when accompanied by high-temperature potassicferrous/magnetite (HT K-Fe) and/or lower-temperature potassic-ferric/hematite-hydrolitic alteration types, polymetallic IOCG mineralisation (Williams et al., 2005) can also be present.

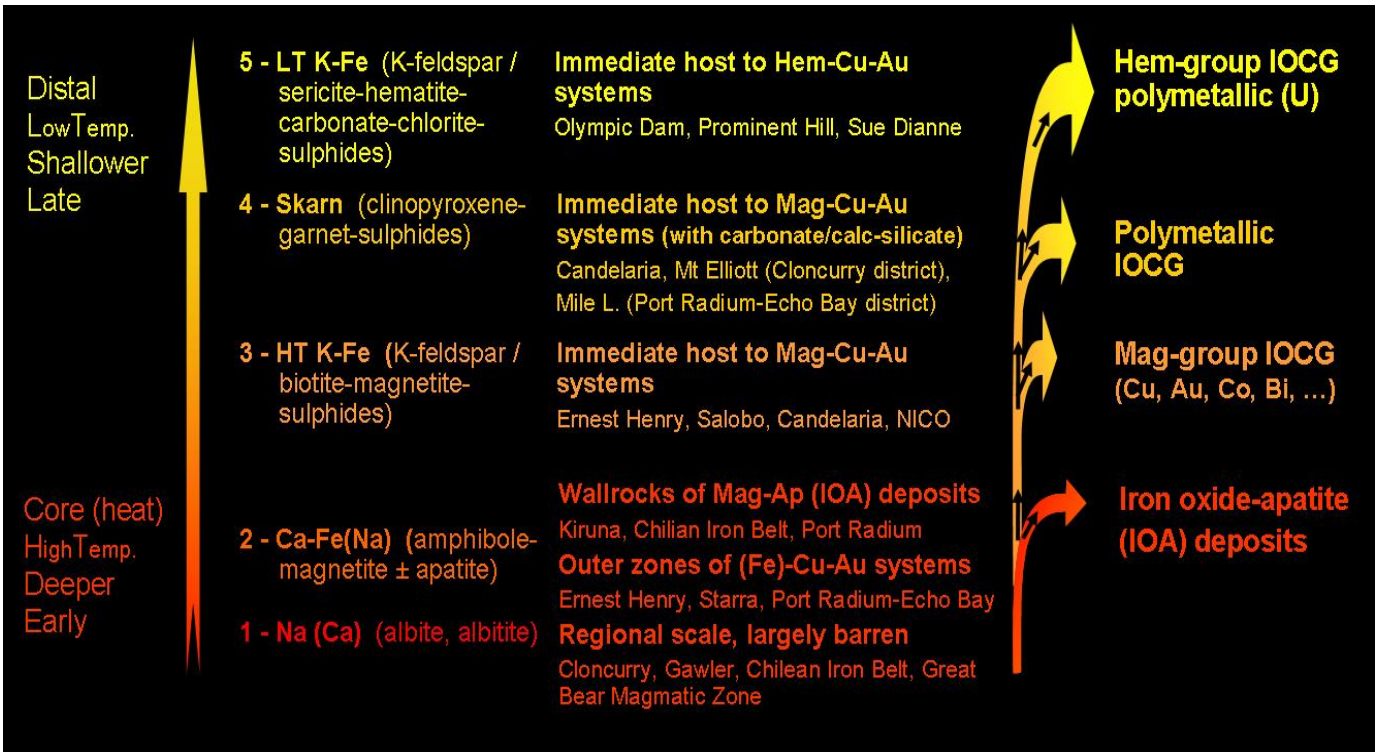

Figure 2. Alteration vector-to-mineralisation model (Corriveau et al. 2010).

Iron oxide copper-gold deposits include a range of hydrothermal mineral deposits that contain copper, with or without gold, as well as abundant magnetite and/or hematite with Fe:Ti ratios greater than those in most igneous rocks and bulk crust. The minerals occur in a spatial continuum dependant on their distance from the core (deeper) zone (Fig. 2). The presence of conductive material such as copper and magnetic minerals indicates that the model can be tested using geophysical methods such as MT and magnetics. In essence, at NICO, the expected response from the model as we move outwards from the core zone is a transition from a low conductivity and susceptibility zone, to a high susceptibility, low conductivity zone and, and finally to a low susceptibility, high conductivity zone.

MT Survey

The MT survey consisted of 32 sites at the NICO camp and employed a rather complex assortment of instrumentation to maximize the amount of data that could be collected by a small crew over an 11 day period. Typically an MT site is comprised of four or five sets of independent measurements of various components of the Earth's natural electric and magnetic fields (Ex, Ey, Hx, Hy and often Hz) with the subscript x designated for horizontal measurements aligned north-south; y, horizontal east-west and z, vertical. As certain induction coils are better suited (i.e. have lower noise floors) in certain frequency bandwidths, data may be re-acquired at a site using a different set of coils. Exploiting the fact that horizontal components of the magnetic field vary more uniformly (spatially) than their electric field counterparts, to save time magnetic measurements were sometimes not acquired at sites if simultaneous magnetic measurements at another nearby site were available. The various instrument configurations used are summarized in Table 1. Each row corresponds to a unique sounding and as such multiple rows can correspond to the same site location. Each sounding could either be E-only (meaning no induction coils were installed) or a mix of E and H, and the coils' identifications corresponding to the x, y and z direction are given. MT coils used to measure magnetic field variations are sensitive to variations in different period bands. Coil IDs in Table 1 beginning with AMTC indicate the coils were designed for so-called audio-magnetotelluric (AMT) bands (approximately 20000 Hz to 20 Hz), whereas MTC coil IDs indicate the coils deployed were optimal for standard MT bands typically between 400 Hz to 1000 s). If only two coil identifications are listed, then the site did not include a vertical coil. If special mention of a coil ID for Hz is given in Table 1, then the site had a vertical coil, but no horizontal coils. In this latter case a site vertical field transfer function (VTF), analogous to the VLF tipper response, can be generated using (simultaneous) measurements by horizontal coils at another site. The VTFs can be modeled simultaneously with the MT response obtained from ratios of E and H fields.

The data were processed using the schemes implemented in the SSMT2000 package (Phoenix Geophysics), and based on method 6 of Jones et al. (1989). The data files used in the processing of each sounding is summarized in Table 2. Each sounding was edited to reduce the effects of outliers in the estimation of impedances, and where soundings at a site were obtained using both AMT and MT coils, the data were merged. In general data quality is excellent (see Figure 7 for example); however the high frequency portion of the data contains two sources of measurement error related to instrumentation. The first is band limited around 2000 Hz (see for example lou014 and lou1019 in Figure 7) and is due primarily to the low strength of ambient magnetic signals at those frequencies (Garcia and Jones, 2002). Not all sites exhibit this bias (e.g. remaining sites plotted in Figure 7), as they were recorded overnight when signal strength is stronger. A second error, discovered post survey, is related to a high order (μs to ms) drift in the timing of one of the recorders utilized in the survey (box 1561). This drift does not affect estimates of the apparent resistivities; however it does affect calculations of the phase at high frequencies (greater than 1000 Hz). Only those sites using box

1561 are affected (Identified in Table 2 by the first four numbers in data file name used in the data processing). These data have been downweighted in the 3-D inversion.

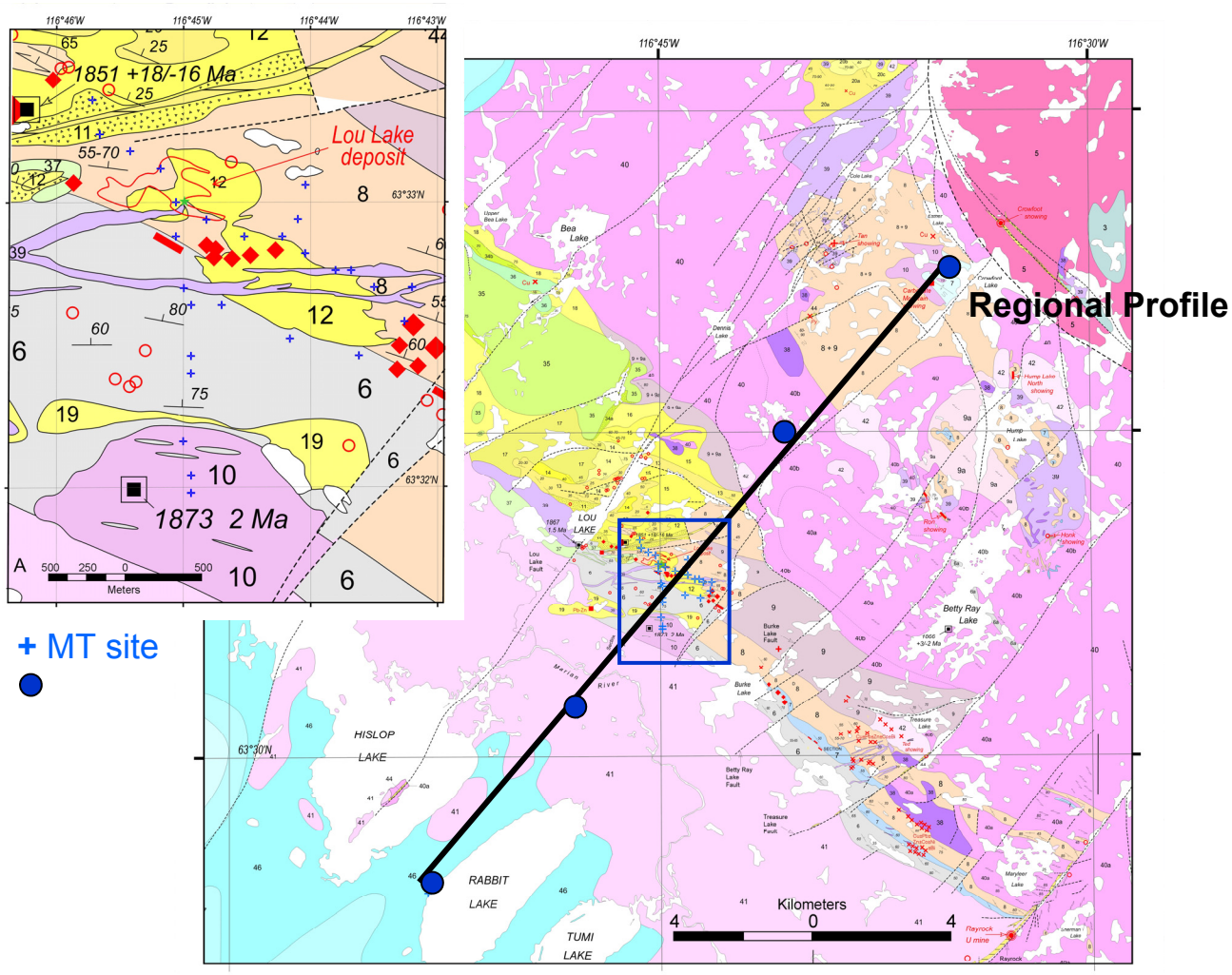

Figure 3. 2010 MT Survey Site Locations. The NICO (also referred to as the Lou Lake deposit) mine-camp scale sites (blue +) is outlined in the inset box and the regional MT sites (blue circles) and line used to project the 1-d inversion results are shown. Red diamonds are mineral showings. Modified after (Ghandhi et al., 1996)

Table 1 List of Soundings and Coordinates of MT sites for the 2010 Survey

Sounding	DATA FILE	INSTALL Date	Location	lat (deg/min)		lon(deg/min)		Latitude	Longitude	Coils or E-only
lou32aa	1562627C	27/06/10	lou032	63	32.479	-116	-44.962	63.541	-116.749	AMTC1170,AMTC1171,none
lou31aa	1562627B	27/06/10	lou031	63	32.323	-116	-44.708	63.539	-116.745	E-only
lou30aa	1562627A	27/06/10	lou030	63	32.428	-116	-44.969	63.540	-116.749	E-only
lou29ma	1562626E	26/06/10	lou029	63	31.963	-116	-44.958	63.533	-116.749	E-only
lou29aa	1562626D	26/06/10	lou029	63	31.962	-116	-44.96	63.533	-116.749	E-only
lou28aa	1562626C	26/06/10	lou028	63	32.032	-116	-44.946	63.534	-116.749	E-only
lou27aa	1562626B	26/06/10	lou027	63	32.164	-116	-45.007	63.536	-116.750	E-only
lou26aa	1562625C	25/06/10	lou026	63	33.363	-116	-45.74	63.556	-116.762	E-only
lou25ma	1464626A	25/06/10	lou025	63	33.231	-116	-45.657	63.554	-116.761	E-only
lou25aa	1562626A	25/06/10	lou025	63	33.231	-116	-45.657	63.554	-116.761	E-only
lou24aa	1561625D	25/06/10	lou024	63	33.153	-116	-45.434	63.553	-116.757	AMTC1170,AMTC1171,AMTC1215
lou23aa	1562625B	25/06/10	lou023	63	33.132	-116	-45.203	63.552	-116.753	E-only
lou22aa	1562625A	25/06/10	lou022	63	33.003	-116	-45.066	63.550	-116.751	E-only
lou21aa	1562624C	24/06/10	lou021	63	32.867	-116	-45.044	63.548	-116.751	E-only
lou20aa	1562624B	24/06/10	lou020	63	32.952	-116	-44.795	63.549	-116.747	AMTC1170,AMTC1171,AMTC1215
lou19aa	1562624A	24/06/10	lou019	63	32.879	-116	-44.502	63.548	-116.742	E-only
lou18ma	1464623A	23/06/10	lou018	63	34.97	-116	-40.64	63.583	-116.677	E-only
lou17ma	1462623B	23/06/10	lou017	63	37.543	-116	-34.874	63.626	-116.581	MTC1400,MTC1401,AMTC1215
lou16ma	1462623A	22/06/10	lou016	63	27.902	-116	-53.103	63.465	-116.885	MTC1400,MTC1401,AMTC1215
lou15ma	1464622C	22/06/10	lou015	63	30.657	-116	-47.905	63.511	-116.798	E-only
lou15ma	1464622B	22/06/10	lou015	63	30.657	-116	-47.905	63.511	-116.798	E-only
lou15ma	1464622A	22/06/10	lou015	63	30.657	-116	-47.905	63.511	-116.798	E-only
lou14aa	1561621B	21/06/10	lou014	63	32.905	-116	-44237	63.548	-116.737	E-only
lou13aa	1561621A	21/06/10	lou013	63	33.043	-116	-44.014	63.551	-116.734	E-only
lou12mc	1464625A	25/06/10	lou012	63	32.951	-116	-44.091	63.549	-116.735	E-only
lou12mb	1562623A	23/06/10	lou012	63	32.95	-116	-44.093	63.549	-116.735	E-only Hz=AMTC1174
lou12ma	1462620B	20/06/10	lou012	63	32.949	-116	-44.088	63.549	-116.735	MTC1400, MTC1401
lou12ab	1561621C	21/06/10	lou012	63	32.957	-116	-44.089	63.549	-116.735	E-only Hz=AMTC1174
lou12aa	1561620B	20/06/10	lou012	63	32.95	-116	-44.089	63.549	-116.735	E-only
lou11ab	1561624A	24/06/10	lou011	63	32.837	-116	-44.056	63.547	-116.734	AMTC1170, AMTC1171
lou11aa	1562621A	20/06/10	lou011	63	32.835	-116	-44.057	63.547	-116.734	AMTC1170, AMTC1171
lou10aa	1561620A	20/06/10	lou010	63	32.755	-116	-43.787	63.546	-116.730	E-only
lou09ma	1462619A	19/06/10	lou009	63	32.681	-116	-43.225	63.545	-116.720	E-only
lou09aa	1562619B	19/06/10	lou009	63	32.683	-116	-43.224	63.545	-116.720	E-only

Sounding	DATA FILE	INSTALL Date	Location	lat (deg/min)		lon(deg/min)		Latitude	Longitude	Coils or E-only
lou08aa	1562619A	19/06/10	lou008	63	32.677	-116	-43.499	63.545	-116.725	E-only but with HZ=AMTC1174
lou07aa	1561619A	19/06/10	lou007	63	32.734	-116	-43.692	63.546	-116.728	AMTC1170, AMTC1171
lou06md	1464620B	20/06/10	lou006	63	32.602	-116	-43.251	63.543	-116.721	MTC1400, MTC1401
lou06mc	1464620A	20/06/10	lou006	63	32.602	-116	-43.251	63.543	-116.721	MTC1400,MTC1401,AMTC1215
lou06mb	1464619A	19/06/10	lou006	63	32.602	-116	-43.251	63.543	-116.721	MTC1400, MTC1401
lou06ma	1464618A	18/06/10	lou006	63	32.602	-116	-43.251	63.543	-116.721	MTC1400,MTC1401,AMTC1215
lou06aa	1561619C	19/06/10	lou006	63	32.607	-116	-43.248	63.543	-116.721	AMTC1170, AMTC1171
lou05mb	1462618A	18/06/10	lou005	63	32.483	-116	-43.639	63.541	-116.727	E-only
lou05ma	1462617B	17/06/10	lou005	63	32.491	-116	-43.639	63.542	-116.727	E-only
lou05ab	1561618A	18/06/10	lou005	63	32.482	-116	-43.64	63.541	-116.727	E-only
lou05aa	1561617A	17/06/10	lou005	63	32.482	-116	-43.64	63.541	-116.727	E-only
lou04ab	1562618A	18/06/10	lou004	63	32.537	-116	-44.183	63.542	-116.736	AMTC1170,AMTC1171,AMTC1174
lou04aa	1562617A	17/06/10	lou004	63	32.537	-116	-44.184	63.542	-116.736	AMTC1170,AMTC1171
lou03ma	1462616A	16/06/10	lou003	63	32.653	-116	-44.71	63.544	-116.745	E-only
lou03aa	1561616A	16/06/10	lou003	63	32.655	-116	-44.698	63.544	-116.745	E-only
lou02aa	1562616A	16/06/10	lou002	63	32.656	-116	-44.941	63.544	-116.749	AMTC1170,AMTC1171
lou01mc	1464617B	17/06/10	lou001	63	32.691	-116	-45	63.545	-116.750	MTC1400,MTC1401
lou01mb	1464617A	17/06/10	lou001	63	32.691	-116	-45	63.545	-116.750	MTC1400,MTC1401
lou01ma	1464616A	16/06/10	lou001	63	32.691	-116	-45	63.545	-116.750	MTC1400,MTC1401

Table 2. Time series (data files) used to generate the Mt responses for all sites.

Site1:

lou01ma

E:	1462616A
Hx,Hy:	1462616A
Hz :	-

lou01mb

E:	1462617A
Hx,Hy:	1462617A
Hz :	-

lou01mc

E:	1462617B
Hx,Hy:	1462617B
Hz :	-

Site 2 :

lou2aa

E:	1562616A
Hx,Hy:	1562616A
Hz :	-

Site 3 :

E:	1462616A
Hx,Hy:	1461616A
Hz :	-

lou03ma

lou03aa

E:	1561616A
Hx,Hy:	1562616A
Hz :	-

Site 4 :

Lou04aa

E:	1562617A
Hx,Hy:	1562617A
Hz :	-

Lou04ab

E:	1562618A
Hx,Hy:	1562618A
Hz :	1562618A

Site 5 :

Lou05ma

E:	1462617B
Hx,Hy:	1464617B
Hz :	-

Lou05mb

E:	1462618A
Hx,Hy:	1464618A
Hz :	1464618A

Lou05aa

E:	1561617A
Hx,Hy:	1562617A
Hz :	-

Lou05ab

E:	1561618A
Hx,Hy:	1562618A
Hz :	1562618A

Site 6 :

Lou06ma

E:	1464618A
Hx,Hy:	1464618A
Hz :	1464618A

Lou06mb

E:	1464619A
Hx,Hy:	1464619A
Hz :	-

Lou06mc

E:	1464620A
Hx,Hy:	1464620A
Hz :	1464620A

Lou06md

E:	1464620B
Hx,Hy:	1464620B
Hz :	-

Lou06aa

E:	1561619C
Hx,Hy:	1561619C
Hz :	-

Site 7 :

Lou07aa

E:	1561619A
Hx,Hy:	1561619A

Hz :	-

Site 8 :
Lou08aa

E:	1562619A
Hx,Hy	1561619B
Hz :	-

Site 9 :
Lou09ma

E:	1462619A
Hx,Hy:	1464619A
Hz :	-

Lou09aa

E:	1562619B
Hx,Hy:	1561619C
Hz :	-

Site 10 :
Lou10aa

E:	1561620A
Hx,Hy:	1562620A
Hz :	-

Site 11 :
Lou11aa

E:	1562621A
Hx,Hy:	1562621A
Hz :	-

Lou11ab

E:	1561624A
Hx,Hy:	1561624A
Hz :	-

Site 12 :
Lou12ma

E:	1462620B
Hx,Hy:	1464620B
Hz :	-

Lou12mc

E:	1464625A
Hx,Hy:	1462625A
Hz :	-

* lou12mb does not exist.

Lou12ab

E:	
Hx,Hy:	
Hz :	

Lou12ac

E:	1562623A
Hx,Hy:	1561623A
Hz :	1562623A

Site 13 :
Lou13aa

E:	1561621A
Hx,Hy:	1562621B
Hz :	-

Site 14 :
Lou14aa

E:	1561621B
Hx,Hy:	1562621B
Hz :	-

Site 15 :
Lou15ma

E:	1464622C
Hx,Hy:	1462623A
Hz :	-

Site 16 :
Lou16ma

E:	1462623A
Hx,Hy:	1462623A
Hz :	1462623A

Site 17 :
Lou17ma

E:	1462623B
Hx,Hy:	1462623B
Hz :	1462623B

Site 18 :
Lou18ma

E:	1464623A
Hx,Hy:	1462623B
Hz :	1462623B

Site 19 :
Lou19aa

E:	1562624A
Hx,Hy:	1561624B
Hz :	-

Site 20 :
Lou20aa

E:	1562624B
Hx,Hy:	1562624B
Hz :	1562624B

Site 21 :
Lou21aa

E:	
Hx,Hy:	
Hz :	

Site 22 :
Lou22aa

E:	1562625A
Hx,Hy:	1561625A
Hz :	1561625A

Site 23 :
Lou23aa

Note : Runtime error during the first processing.
Reprocessed by terminating 1561625B at
19:42:42.

E:	1562625B
Hx,Hy:	1561625B
Hz :	1561625B

Site 24 :
Lou24aa

E:	1561625C
Hx,Hy:	1561625C
Hz :	1561625C

Site 25 :

Lou25ma

E:	1464626A
Hx,Hy:	1462625A
Hz :	-

Lou25aa

E:	1562626A
Hx,Hy:	1561625D
Hz :	1561625D

Site 26:
Lou26aa

E:	1562625C
Hx,Hy:	1561625D
Hz :	1561625D

Site 27:
Lou27aa

E:	1562626B
Hx,Hy:	1561626A
Hz :	-

Site 28:
Lou28aa

E:	1562626C
Hx,Hy:	1561626A
Hz :	-

Site 29:
Lou29aa

E:	1562626D
Hx,Hy:	1561626A
Hz :	

Lou29ma

E:	1562626E
Hx,Hy:	1462625A
Hz :	

Note: lou29ma could not be processed due to an unknown error in processing code.

Site 30:
Lou30aa

E:	1562627A
Hx,Hy:	1561627A
Hz :	-

Site 31:
Lou31aa

E:	1562627B
Hx,Hy:	1561627A
Hz :	-

Site 32:
Lou32aa

E:	1562627C
Hx,Hy:	1562627C
Hz :	-

One and Two Dimensional Analyses

Following data editing, preliminary models were generated using robust 1-d inversion techniques. Due to the finite bandwidth and measurement errors, multiple models can fit the data. Thus some external constraints were applied. The Occam inversion code (Constable et al., 1987) was used to generate 1-D layered earth models at each site. The Occam approach minimizes gradients in model

structure to constrain model selection, in addition to being a stable and robust algorithm, converging on the target misfit in a relatively small number of iterations. No additional constraints were used to stabilize the inversion. To minimize the effects of lateral changes in structure, the apparent resistivities and phases calculated from the geometric average of the impedance tensor were used as the input for the inversion. For most sites the inversion was robust and produced a good fit to the data within 10 iterations. The inversion results along two profiles were contoured.

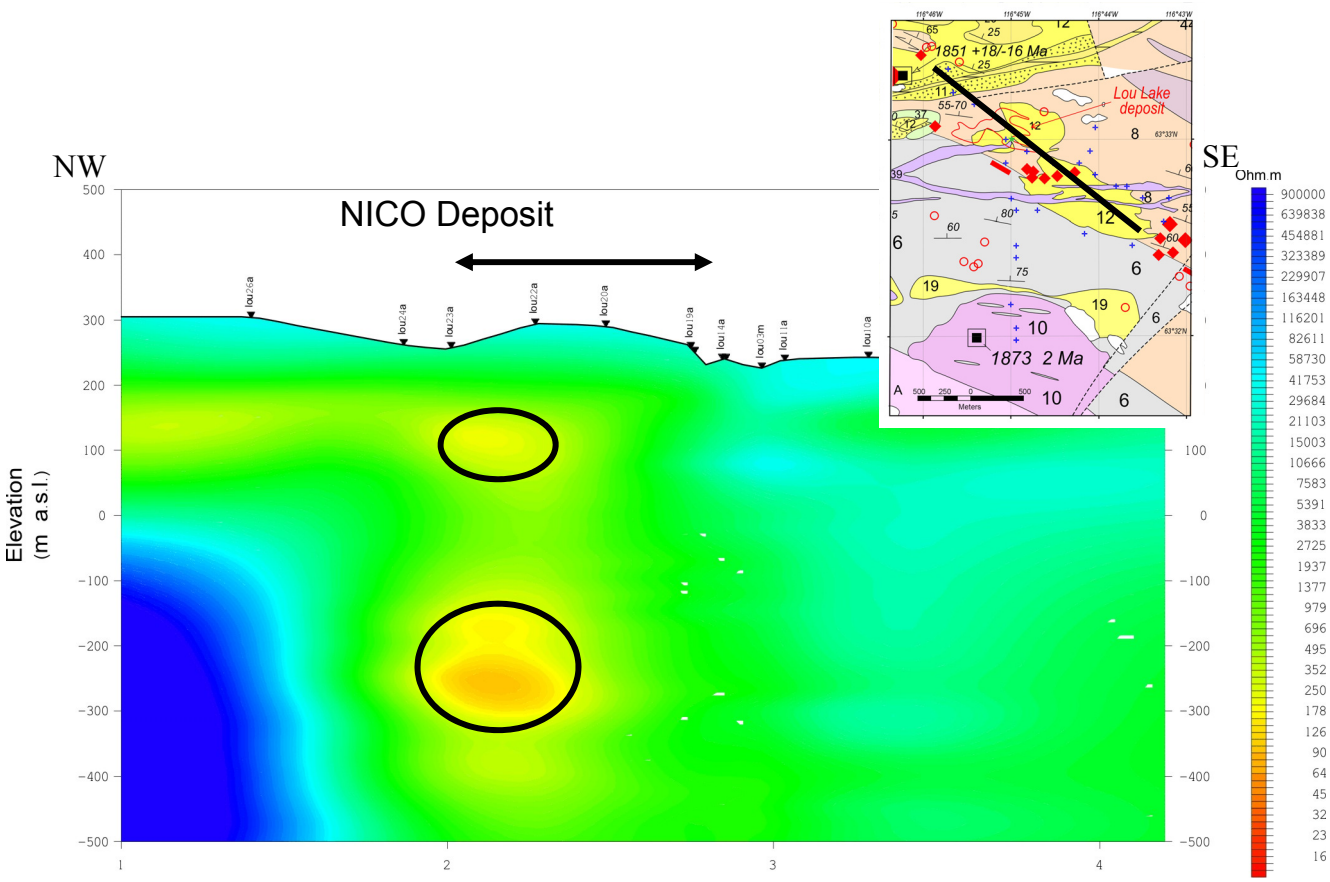

Figure 4 1-D Inversion results, smoothed and contoured and projected along a NW-SE line shown in the inset.

MT resolution is higher in the shallower section (Figure 4) due to the increased sensitivity of the higher frequency data to smaller scale structure. The background resistivity is dominated by relatively high values; however two resistivity lows (i.e. conductivity highs=yellow) in the vicinity of the NICO deposit can be identified. This section must be interpreted with caution as all structure in a 1-D inversion model is inserted directly below the MT sites, and broadside or off-profile affects may be mis-located or false conductors may be introduced. Two or three dimensional modeling should be employed to better locate important structures.

Higher frequency electromagnetic (EM) fields do not penetrate as deeply into the earth as long period waves. Therefore the resolution of MT results decreases with depth. To highlight structures at depth, a second 1-D inversion model (Figure 5) along the NE-SW regional profile (Figure 3). The key element in Figure 5 is the possible existence of a low resistivity region (labeled “Conduit?”) dipping southwest below the deposit to upper mantle depths. As with the shallower section caution should be exercised in interpreting the image due to possible mislocations of structure and broadside effects.

SW NE

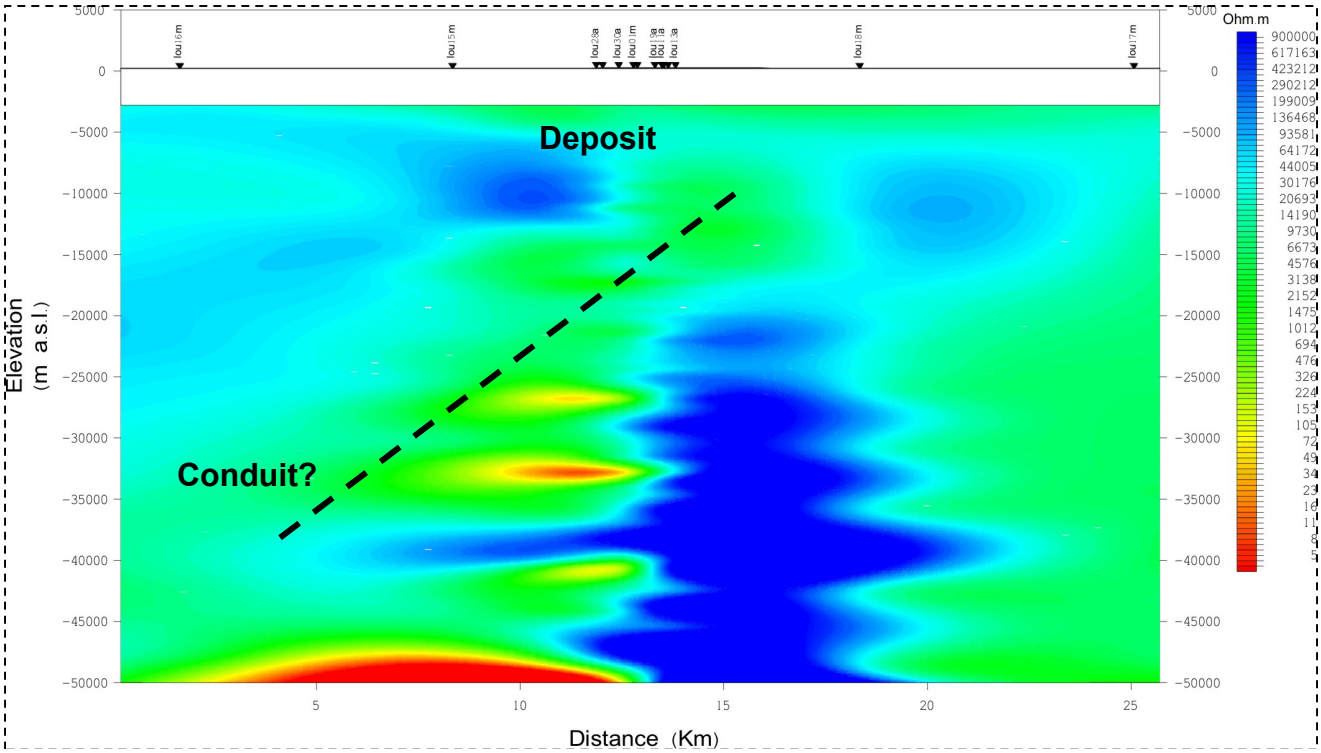

Figure 5. Contoured 1-D inversions along the Regional line shown in Figure 3.

In general, due to computer memory limitations, 2-D models can be run with considerable more parameters than 3-D models and may therefore afford better resolution than 3-D algorithms; however they can be hampered by broadside effects, so must be used with caution. To determine if 2-D or 3-D modeling is required, it is common to ascertain the dominant electrical fabric direction (strike-direction) inherent to the MT data (e.g., Spratt et al., 2011). If the electrical fabric demonstrates reasonable spatial uniformity then it is reasonable to do a 2-D inversion of the data. A multi-directional fabric suggests that 3-D techniques should instead be used. The electrical fabric (strike-direction), calculated using the algorithm of McNeice and Jones (2006) for a frequency of 10 Hz corresponding to upper crustal depths, is shown in Figure 6. Within the inset area (see Figure 3 for location of inset) a sector diagram (Figure 6) is used to identify patterns, whereas at regional sites individual strike directions are plotted. The strike directions demonstrate a reasonable degree of uniformity over the entire dataset and the dominant direction aligns subparallel the primary brecciation direction (~120°, Montreuil et al., 2010) related to early, core, stages of the Corriveau et al.(2010) alteration vector-to-mineralisation model. However we have opted to do 3-D inversions in order to increase the accuracy of the electrical structure at the expense of some model resolution to address the key goal of indentifying spatial relationships amongst the MT, geological and magnetic models for the NICO mine camp.

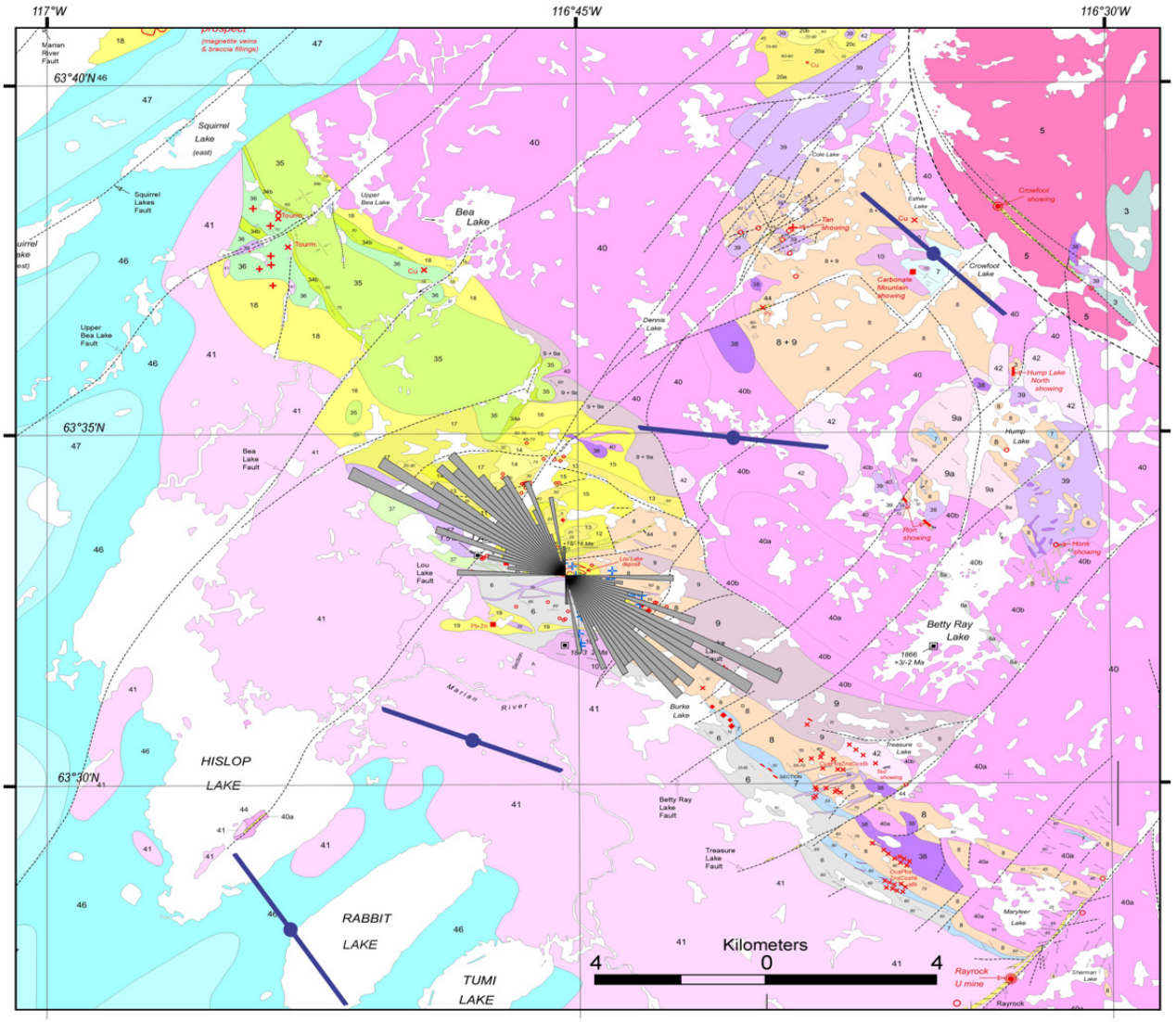

Figure 6. Strike directions shown as a sector diagram (grey lines) for the inset area, and as individual strikes (blue lines) for the regional sites.

Preliminary 3-D Modeling

MT

The 3-D inversion technique utilized in this study (Sirivaraporn et al., 2009) is also based on the conservative Occam principal used in the 1-D analysis. The algorithm is particularly useful as 1) it also uses the vertical field measurements at each site where available; helpful in the discrimination of closely spaced conductors, and 2) has been programmed to run on multi-cpu clusters that enable typical run-times of days rather than weeks or months. In general the fit of the final 3-D MT model to the data is quite good (Figure 7) with an overall normalized RMS of 1.87. As stated earlier, weights at the high frequencies have been decreased and indeed one can see that the resistivities have been better fit, in contrast to the phases which are suspect due to the timing error mentioned earlier. It must be remarked that the data are quite complicated relative to other datasets; however the character of the data are well fit. A few novel strategies employed were instrumental in achieving this high degree of

fit. Firstly, the model mesh (see Figure 8) was rotated to be parallel and orthogonal the 120 degree strike. This should allow the EM fields within the model to be calculated more accurately. Secondly, the model discretization (i.e. mesh) was set up using non-uniform cells size. Cell sizes away from sites were allowed to increase in size where possible. In addition, cell sizes varied in a uniform manner with $\log_{10}$ depth. This strategy enabled more cells to fit in memory and enabled a reasonable balance of model resolution and run-time. The final strategy employed was to downweight data outliers such as those related to the easily identifiable noise sources discussed earlier. In addition, as is common in MT inversion, data errors were assigned floors of 5%.

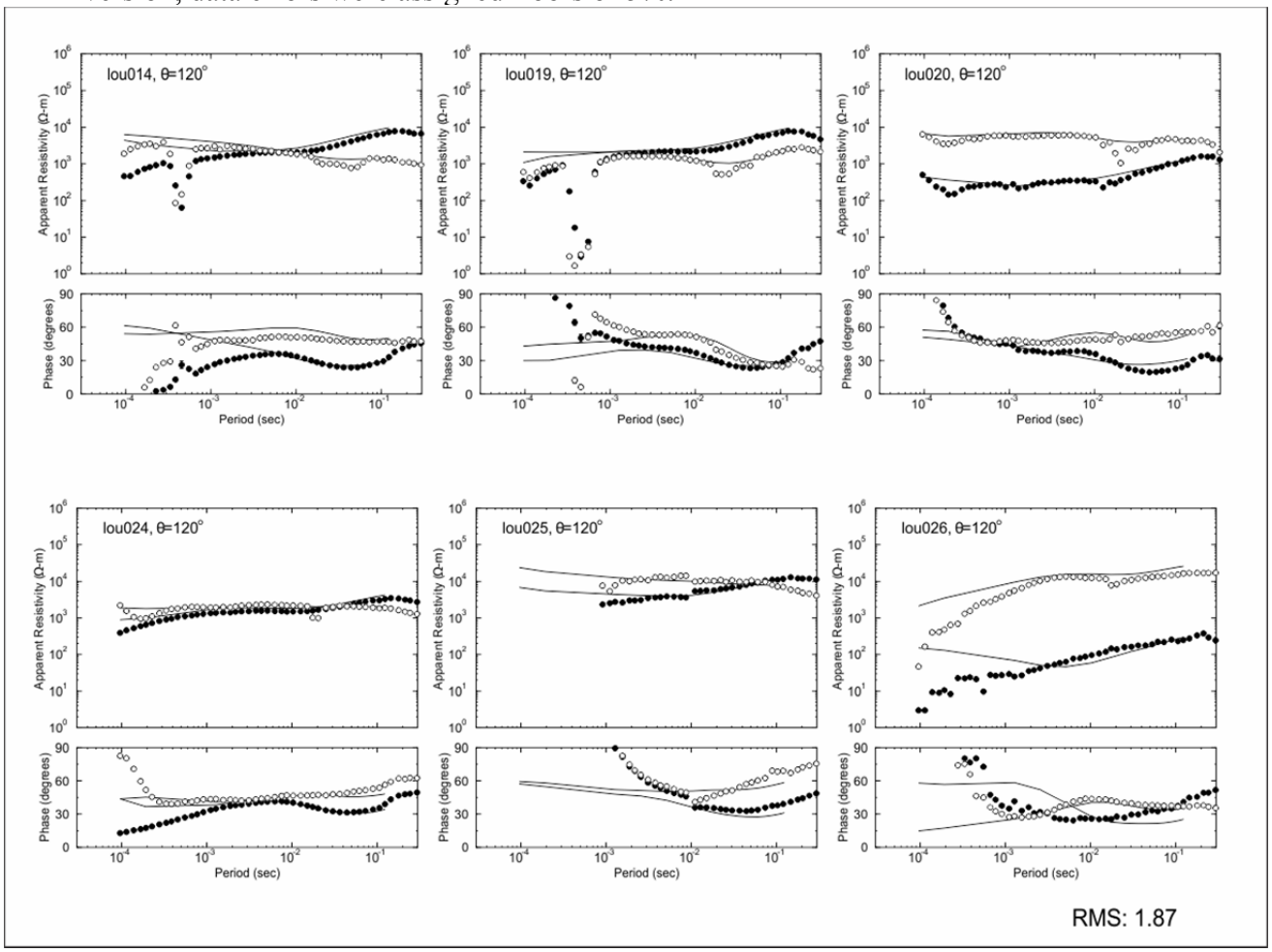

Figure 7. MT data (symbols) at six sites and fit curves generated from the 3-D model in Figure 8. Open circles are the XY response calculated from Ex and Hy. Black circles are the YX response calculated from Ey and Hx.

Two slices from the model are shown in Figure 8 andFigure 9. Features in the horizontal slice in Figure 8 can be correlated to the inset geological map using the site locations. Some of the conductive features in the model are beneath sites and some significant ones are not. The resistivity low at 250m depth and at Y = -500m in the vertical slice in Figure 9 is likely the NICO deposit. As suggested by the 1-D models this feature may be related to a second feature ("A") at depths as great as 1 km and it in turn may be related to another conductive feature ("B") at Y=0 however this feature is inferred to exist by data at sites some distance away and must therefore be treated with caution.

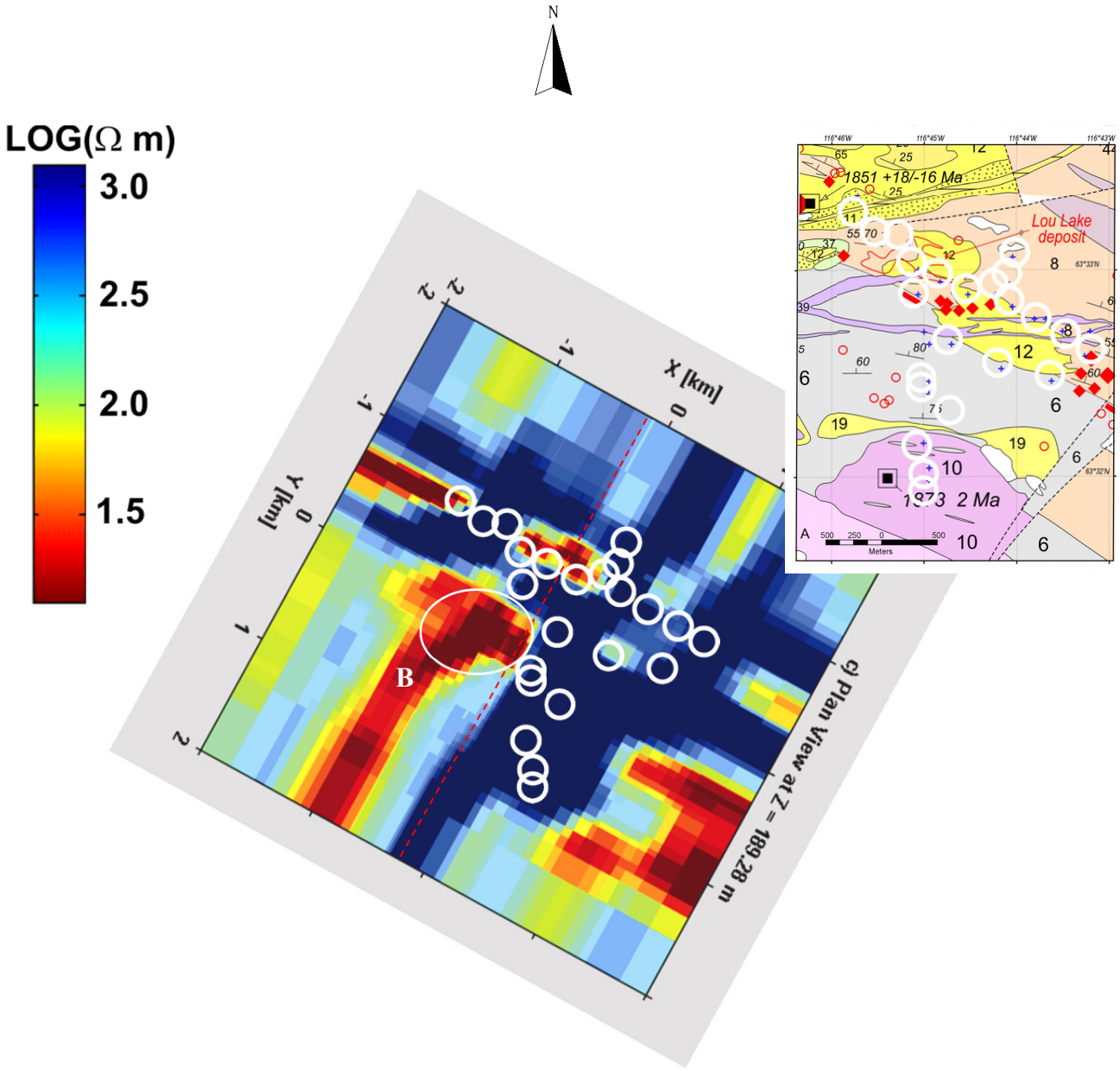

Figure 8. Slice at 189 m of the 3-D model showing site locations. Feature B and red dashed line shows surface trace of the vertical slice presented in Figure 9. Feature B Figure 9 in is also shown. Feature B is along strike of the brecciation observed by Montreuil et al. (2010).

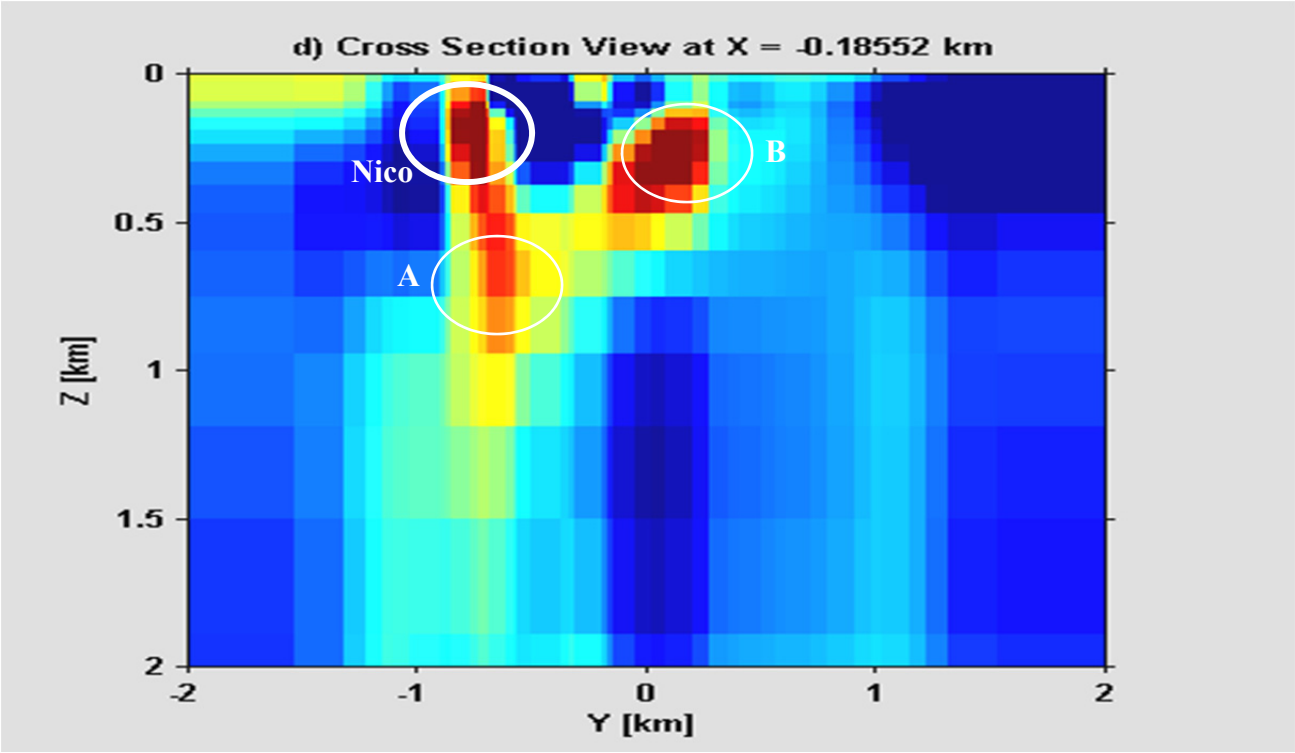

Figure 9. Vertical slice through model at approximate location of NICO deposit. Features A and B are discussed in the text. Colour scale same as Figure 8.

Magnetics

A 3-D magnetic inversion model was constructed for the study area in order to investigate the variation of magnetic susceptibility in the area of the NICO deposit and to enable a spatial comparison of magnetic and electromagnetic physical properties.

High-resolution aeromagnetic data for this study was constructed from a regional compilation of aeromagnetic data (Hayward and Oneschuk, 2011) and proprietary data. In the study area this includes high-resolution data from the NICO deposit (Pritchard, 1995) (Line spacing 100 m, elevation 100 m), the Mazenod Lake survey (Line spacing 500 m, elevation 120 m), and regional data acquired by the geological survey of Canada (Figure 10). A 3-D magnetic inversion model for the NICO was calculated using the Data Space Inversion Magnetics 3D (DSIM3D) software (Pilkington 2009). Aeromagnetic data for the NICO area was gridded at 50 m and upward continued by 200 m to decrease high-frequency noise, in Oasis Montaj. A 512x512x128 mesh of 50 m cubic cells was constructed for the NICO region with padding around the region of interest (UTM 506200/526150/7035500/7055450). The run-time for the inversion was approximately 1 week.

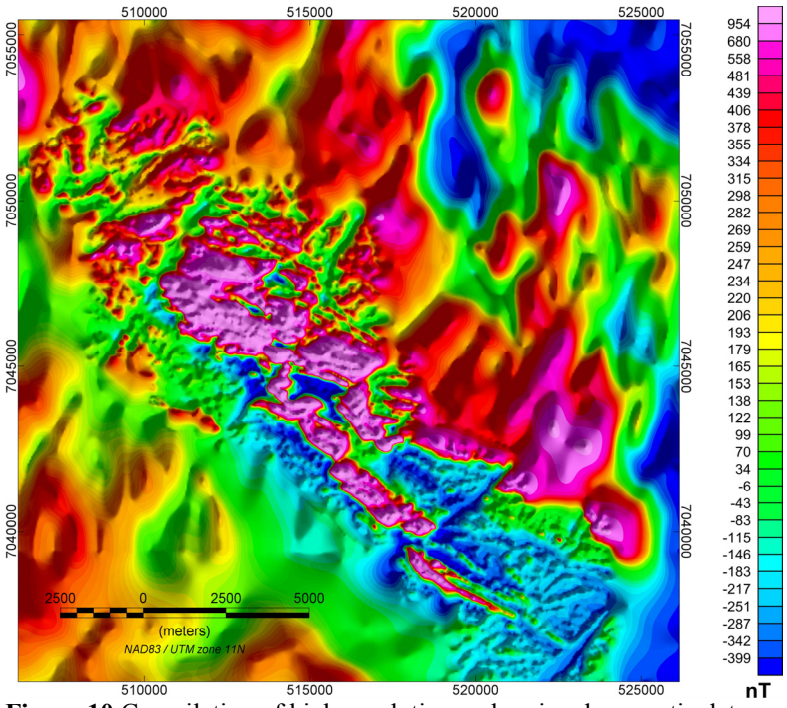

Figure 10 Compilation of high-resolution and regional magnetic data used in the calculation of the 3-D magnetic inversion model for the region of the NICO deposit.

Magnetic inversion assumes a purely induced source for the magnetic anomalies and cannot account for the effects of the natural remanent magnetization (NRM). For 80% of the 285 rocks sampled and measured in the GBmz (Figure 11), the NRM is smaller than the induced magnetization. The direction of the NRM was measured (with an AGICO JR5-A spinner magnetometer) for 39 sites of ~6 samples per site from the NICO area. All but one site hold downward and usually steeply down remanent inclination directions (mean = 68.5°) near to that of the present external magnetic field (82°). As the NRMs are in a broadly similar direction to the geomagnetic field, and the magnitude is roughly proportional to the susceptibility, the presence of rocks with high remanence would likely increase the magnitude of the observed magnetic anomalies. This may result in an overestimate of the susceptibility in model calculations, but will not significantly affect the broad shape of the predicted magnetic sources.

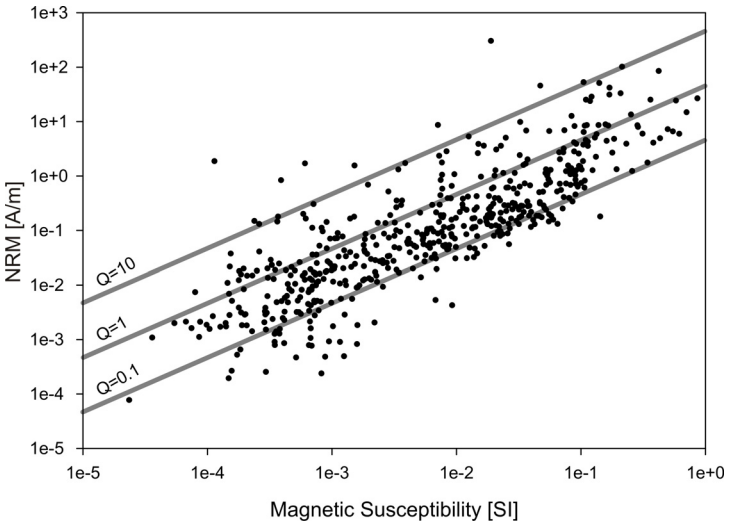

Figure 11 Relationship between magnetic susceptibility and natural remanent magnetisation (NRM) for samples from the GBmz, with respect to lines of equal Koenigsberger ratio, Q. 80% of samples have Q<1, indicating that induced magnetization dominates over remanence as sources for aeromagnetic anomalies.

The magnetic inversion model (Figure 12) suggests that a magnetic source with a magnetic susceptibility of ~ 0.2 – 0.4 SI occurs near to the surface at the NICO deposit and dips steeply towards the NE, continuing to a depth of ~750 m. A deeper and larger magnetic source just to the NE of the NICO deposit, which also dips steeply toward the NE, is also predicted at depths of ~ 800 – 1700 m.

3-D Visualization and integration

One of the goals of the MT survey was to assess the validity of the Corriveau et al.(2010) alteration vector-to-mineralisation model from a geophysical perspective. The metallogenic model predicts a spatial pattern in the alteration that should be visible in the magnetic and electromagnetic models (see Table 3 for the link we are between model minerals and expected geophysical response) and which can be tested through 3-D visualization of the geological and geophysical models. The geological and geophysical models were imported into a GoCAD model space using the Mira Geoscience mining importers toolset (http://www.mirageoscience.com/software/gocad_mining_suite/) and splined using the Sparse toolset (de Kemp 1999). The geophysical models were splined in 3-D to make representations that can be contoured and shaded using iso-surfaces. Care had to be made splining the MT model due to the use of an irregular rectilinear mesh in the formulation of the MT model. Isosurfaces for susceptibility and conductivity were created and shaded as shown in Figure12. The results of the 3-D visualization are provided using the 3-D extensions of the PDF format. This document must be viewed using Adobe® Reader® 9 or later to see the model in 3-D (i.e. the model can be "grabbed" and rotated like objects in a CAD program for better views of spatial relationships). The alteration patterns are not incorporated in this model however the early albitization is associated with the brecciation and faulting and is identified in Figure13. The primary zone of albitization is geophysically blank. As one moves northwest towards the NICO deposit the first region cross is magnetic, and the second zone is conductive, in agreement with the Corriveau et al. (2010) alteration vector-to-mineralisation model (Figure 2).

Table 3 Geophysical Responses Expected at NICO

Mineralization	*Magnetic Response*	*Conductive Response*
albite	nil	nil
Ca-Fe/IOA	yes	nil
HT K-Fe	weak	yes

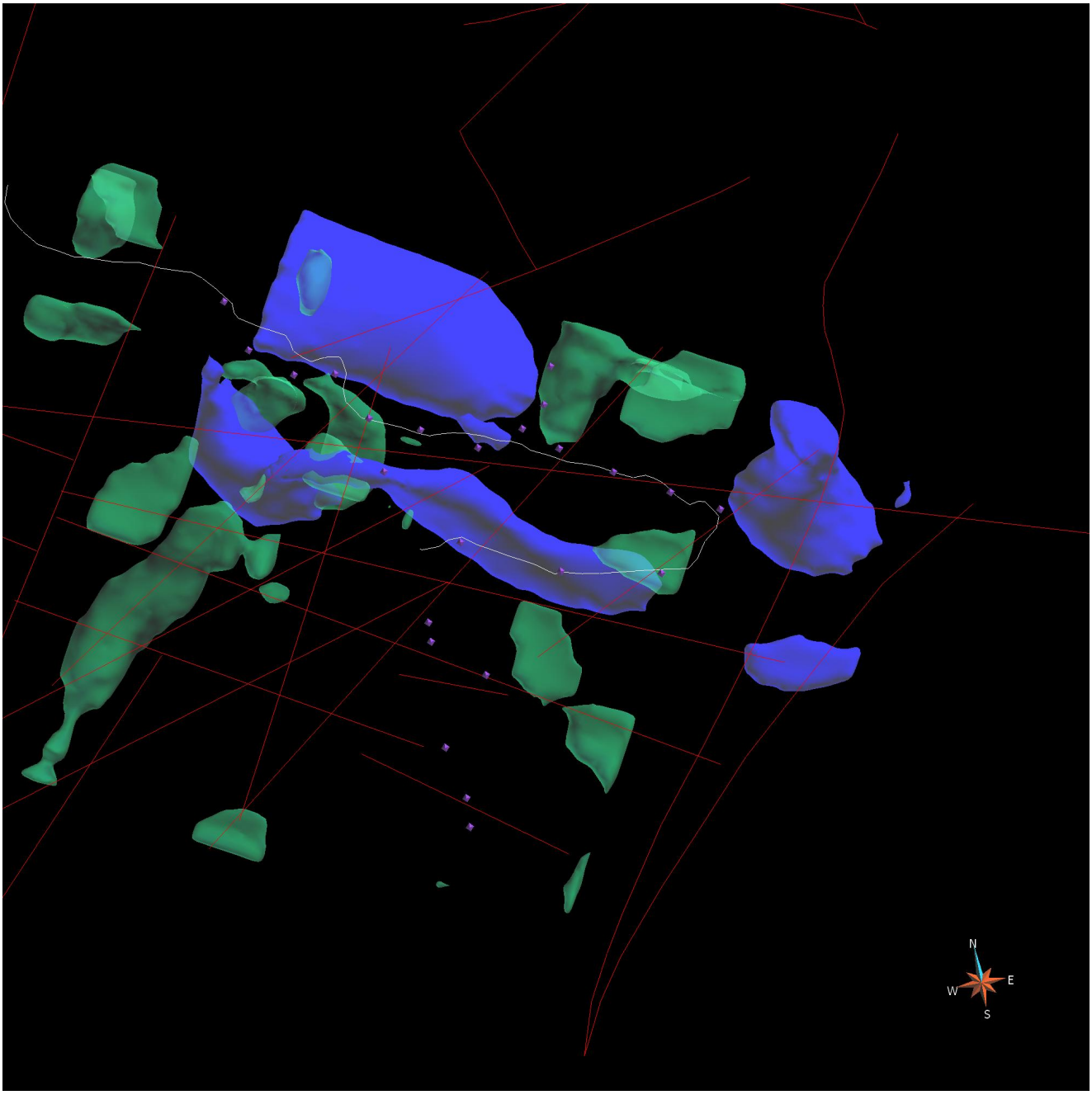

Figure 12 3-D Model. Purple dots are MT site locations. The white line is the mine access road. Red lines are major faults. Purple volumes are regions with k>0.2. Green regions highlight volumes where conductivity is > 0.07 S/m.

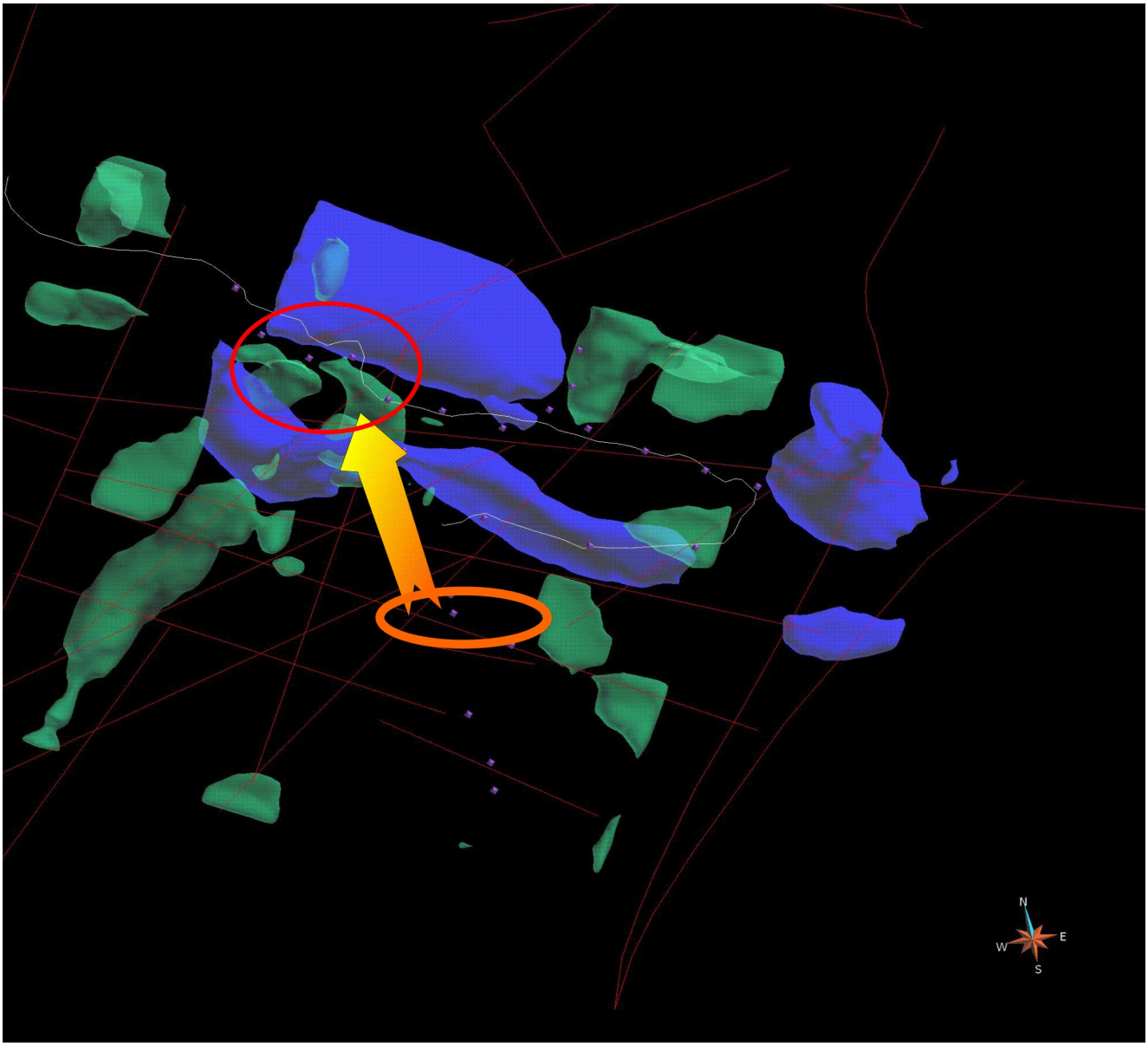

Figure 13 Plan view of 3D model showing trend of alteration (arrow) from the albitization and brecciation (orange circle) to the NICO deposit (red circle).

Discussion

A hypothesis based on the Corriveau et al. (2010) alteration vector-to-mineralisation model suggests a spatial relationship in geophysical responses should be observed at mineralisation showings where the model is applicable. As part of a test of this hypothesis an MT survey was conducted across the NICO deposit. To properly locate the conductive material in space a 3-D inversion of the MT data was eprfomred and compared with a 3-D magnetic inversion. The MT inversion showed a number of interesting features one of which is a shallow conductor related to the NICO deposit itself. This conductor and its spatial relationships with the features in the magnetic model confirm the Corriveau et al. (2010) alteration vector-to-mineralisation model model. The deeper features and the correlation with the albitization and brecciation are speculative but suggest a polycyclic nature to the mineralization. The regional MT line will be discussed in more detail in another paper, but preliminary indications of a deep-seated conduit are observed.

Acknowledgements

The authors would like to thank Fortune Minerals for hosting us and providing a field vehicle and occasional field hand. Eric deKemp was very helpful with GoCAD. J.-F. Montreuil provided the geology shape files used in the GoCAD model. Randy Enkin and various students as part of the GEM Great Bear project are thanked for enthusiastic field help. The comments and review by David Snyder improved this manuscript.

References

Constable, S.C., Parker, R.L., and Constable, C.G. 1987. Occam's inversion: a practical algorithm for generating smooth models from electromagnetic sounding data. Geophysics, 52(3): 289–300.

De Kemp, E.A., 1999, Visualization of complex geological structures using 3-D Bézier construction tools,Computers and Geosciences, 25 (5), pp. 581-597.

Garcia, X., and Jones, A.G. 2002. Atmospheric sources for audiomagnetotelluric (AMT) sounding. Geophysics, 67(2): 448–458.

Gandhi, S.S., Prasad, N., Charbonneau, B.W., 1996. Geological and geophysical signatures of a large polymetallic exploration target at Lou Lake, southern Great Bear magmatic zone, Northwest Territories. Geological Survey of Canada Current Research 1996-E, 147–158.

Groom, R.W., and R.C. Bailey, 1989: Decomposition of magnetotelluric impedance tensors in the presence of local three-dimensional galvanic distortion; Journal of Geophysical Research, v. 94, p. 1913 – 1935.

Hayward, N., Oneschuk, D., 2011. Geophysical series, regional geophysical compilation project, Great Bear Magmatic Zone, Northwest Territories and Nunavut, NTS 85 M and N, and 86 C, D, E, F, K and L. Geological Survey of Canada, Open File, 6835/NTGO Open File 2011-05.

Hildebrand, R.S., Hoffman, P.F., Bowring, S.A., 2010, The Calderian orogeny in Wopmay orogen (1.9 Ga), northwestern Canadian Shield, Bulletin of the Geological Society of America, 122 (5-6), pp. 794-814.

Johnson, J.P., and McCulloch, M.T., 1995, Sources of mineralising fluids for the Olympic Dam deposit (South Australia): Sm-Nd isotopic constraints: Chemical Geology, v. 121, p. 177–199.

Jones, A.G., Chave, A.D., Auld, D., Bahr, K. and Egbert, G., 1989: A comparison of techniques for magnetotelluric response function estimation; Journal of Geophysical Research, v. 94, p. 14,201 – 14,213.

McNeice, G.W., and A.G. Jones, 2001: Multisite, multifrequency tensor decomposition of magnetotelluric data; Geophysics, v. 66, p. 158 – 173.

Montreuil, J –F, Pelleter, E, van Breemen, O, Davis, W, Kerswill, J, Behnia, P, Corriveau, L, ,2009, in, 37th annual Yellowknife Geoscience Forum, , Yellowknife Geoscience Forum Abstracts Volume vol. 2009, p. 83-84

Montreuil, J -F; Corriveau, L; Ootes, L; Jackson, V; Gélinas, L -, 2010, Breccias as markers of tectono-hydrothermal evolution of iron oxide-bearing hydrothermal systems in the Great Bear Magmatic Zone in, 38th annual Yellowknife Geoscience Forum, Yellowknife Geoscience Forum Abstracts Volume 2010, p. 85-86

Pilkington, M., 2009. 3D magnetic data-space inversion with sparseness constraints. Geophysics, 74, L7-L15.

Potter, E G., Montreuil, J –F, Corriveau, L, and DeToni, A., 2013 Geology and hydrothermal alteration of the Fab lake region, Northwest Territories Geological Survey of Canada, Open File 7339; 26 pages (1 sheet), doi:10.4095/292562

Pritchard, R.A., 1995. Dighem survey for Fortune Minerals Limited NICO/Olympic Dam properties, N.W.T. NTS 85N/7, 10, 15. Report 1222-B.

Ranganayaki, R.P. 1984An interpretative analysis of magnetotelluric data. Geophysics, 49, 1730–1748.

Siripunvaraporn, W. and Egbert, G. 2009. WSINV3DMT: Vertical magnetic field transfer function inversion and parallel implementation. Physics of the Earth and Planetary Interiors, 173, 317-329.

Snyder, D.B., 2008. Stacked uppermost mantle layers within the Slave craton of NW Canada as defined by anisotropic seismic discontinuities, Tectonics, 27, doi:10.1029/2007TC002132.

Spratt, J.E., Snyder, D.B. and Craven, J.A., 2011. A magnetotelluric survey across the Committee Bay belt and Rae craton in the Churchill province of Nunavut; Geological Survey of Canada, Open File 6825, 28 p.